

# Stochastic Virtual Power Plant Dispatch via Temporally Aggregated Distributed Predictive Control with Performance Guarantees

Luca Santosuosso, *Member, IEEE*, Fei Teng, *Senior Member, IEEE*, and Sonja Wogrin, *Senior Member, IEEE*

**Abstract**—This paper addresses the energy dispatch of a virtual power plant comprising renewable generation, energy storage, and thermal units under uncertainty in renewable output, energy prices, and energy demand. The nonlinear dynamics and multiple sources of uncertainty render traditional stochastic model predictive control (MPC) computationally intractable as the dispatch horizon, scenario set, and asset portfolio expand. To overcome this limitation, we propose a novel controller that seamlessly integrates MPC with time series aggregation and distributed optimization, simultaneously reducing the temporal, asset, and scenario dimensions of the problem. The resulting controller provides a rigorous performance guarantee through theoretically validated bounds on its approximation error, while leveraging dual information from previous MPC iterations to adaptively optimize the temporal aggregation. Numerical results show that the proposed controller reduces runtime by over 50% relative to traditional stochastic MPC and, crucially, restores tractability where the full-scale dispatch model proves intractable.

**Index Terms**—Stochastic model predictive control, distributed model predictive control, time series aggregation, performance guarantees, virtual power plant dispatch

## I. INTRODUCTION

### A. Literature Review

THE global pursuit of carbon neutrality has accelerated the widespread integration of distributed energy resources (DERs), including variable renewable energy sources (vRES), energy storage systems (ESSs), and flexible loads, into modern power systems. In this context, virtual power plants (VPPs) provide a structured framework for aggregating large populations of DERs into a unified portfolio and coordinating their operation as a single entity [1], enabling efficient participation in energy trading [2] and the provision of grid services [3].

Although the potential of VPPs to enhance the flexibility of modern power systems is widely recognized [4], their operation remains a complex, multi-stage process encompassing long-term planning, short-term scheduling, and real-time dispatch [5]. This paper focuses on the latter stage of this decision-making process.

The real-time energy dispatch of a VPP is commonly formulated as an optimal control problem [6], in which operations are controlled at sub-hourly resolution to optimize a performance criterion, such as minimizing generation costs, while satisfying the technical constraints of DERs. Model predictive control (MPC) has emerged as a widely adopted

approach for this task, owing to its capacity to anticipate system dynamics, explicitly enforce constraints, and iteratively update control actions based on real-time measurements [7].

As VPP operations are affected by multiple sources of uncertainty, such as energy demand, vRES generation, and market prices, previous research has focused on incorporating methods to handle stochasticity within MPC schemes. Traditional deterministic MPC assumes perfect knowledge over the optimization horizon [8], an assumption that is often unrealistic. To address this limitation, alternative control schemes have been investigated: scenario-based stochastic MPC [9], which employs scenarios to represent potential uncertainty realizations; robust MPC [10], which presumes that uncertainty is confined within a predefined set; and chance-constrained MPC [11], which enforces probabilistic guarantees on constraint satisfaction under stochastic variations. A comprehensive review of these methods is provided in [12].

Constraining uncertainty to a finite set, as in robust MPC, is often impractical for unbounded sources such as market prices and may result in excessively conservative solutions [13]. Chance-constrained MPC typically requires explicit reformulations to enforce probabilistic constraints, which often entail significant mathematical complexity and may also introduce conservatism. Scenario-based stochastic MPC is therefore typically preferred due to its flexibility and its ability to represent diverse uncertainty sources. However, as the size and heterogeneity of the VPP portfolio increase, the underlying uncertainty space expands accordingly, potentially requiring a prohibitively large number of scenarios and rendering the MPC scheme computationally intractable.

Notably, beyond increasing with the number of scenarios, i.e., the *scenario dimension* of the control problem, the computational complexity of stochastic MPC also grows with the number and heterogeneity of DERs within the VPP, i.e., its *asset dimension* [14]. Ensuring simultaneous scalability with respect to both dimensions is therefore essential to enable fast real-time dispatch of complex, large-scale VPPs [15].

To this end, prior research has investigated mathematical decomposition methods for deriving distributed MPC schemes that partition the centralized control problem into concurrently solved subproblems, while preserving convergence to global optimality [16]. Within this line of work, various distributed MPC schemes have been proposed, including those based on dual decomposition [16], Douglas–Rachford splitting [17], optimality condition decomposition (OCD) [18], analytical target cascading (ATC) [10], approximate Newton direction methods [19], and the widely used alternating direction method of multipliers (ADMM) [20]. Among these, ADMM and its variants [21] have gained widespread adoption due to their

Luca Santosuosso and Sonja Wogrin are with the Institute of Electricity Economics and Energy Innovation, Graz University of Technology, and the Research Center ENERGETIC, 8010 Graz, Austria (e-mail: luca.santosuosso@tugraz.at; wogrin@tugraz.at).

Fei Teng is with the Department of Electrical and Electronic Engineering, Imperial College London, SW7 2BU London, U.K. (e-mail: f.teng@imperial.ac.uk).

flexibility in handling diverse problem formulations and their well-established convergence properties [22].

Notably, while several studies have distributed computations across either the scenario [23] or the asset [24] dimension of VPP optimization models independently, few have addressed both simultaneously [25]. Crucially, none of these studies addresses scalability across the third complexity dimension of the problem, namely its *temporal dimension*, thereby leaving substantial potential for reducing the computational burden of MPC schemes unexploited. This occurs because temporal decomposition decouples the intertemporal constraints of the original model, producing subproblems that are inherently more challenging to coordinate toward convergence than those resulting from decompositions across assets or scenarios [18].

To alleviate the computational burden associated with the temporal dimension of energy optimization models, time series aggregation (TSA) methods have emerged as a highly effective alternative to decomposition methods. By compacting the full-scale optimization model, TSA produces an aggregated model defined over a reduced set of representative time periods (or clusters), while aiming to preserve the essential temporal dynamics of the original formulation [26]. Unlike decomposition methods, which aim at reducing computational complexity via parallelization, TSA seeks the same objective through a dimensionality reduction of the original optimization model.

Traditional *a priori* TSA methods typically employ standard clustering techniques, such as k-means [27], k-medoids [28], and hierarchical clustering [29], to construct temporally aggregated models based solely on the statistical features of the input time series. More recently, *a posteriori* TSA has emerged as an alternative paradigm, augmenting the clustering procedure with features derived from the optimization model itself, such as insights from previous optimization runs, to yield aggregations that more accurately capture the temporal dynamics of the original full-scale optimization model [30]. Remarkably, a posteriori TSA has the potential to achieve **exact** temporal aggregation [31], yielding an aggregated model that faithfully replicates the output of its full-scale counterpart while delivering substantial computational savings.

While many studies have proposed TSA methods for large-scale energy optimization models [32], particularly for those involving intertemporal constraints that complicate the TSA procedure by requiring the preservation of temporal chronology [33], research on integrating TSA within MPC schemes remains scarce [34]. Notably, none of the existing studies investigates the potential of emerging a posteriori TSA methods to reduce the temporal dimension in stochastic MPC.

Furthermore, since TSA yields an aggregated model that approximates its full-scale counterpart, it is essential in practical applications to provide *performance guarantees* by quantifying the approximation error introduced through temporal aggregation. While formal guarantees have been established for linear programming (LP) [35], mixed-integer linear (MILP) and mixed-integer quadratic programming (MIQP) problems [36], these theoretical results are not readily extendable to quadratic programming (QP) and quadratically constrained quadratic programming (QCQP) formulations, which are commonly employed in the energy dispatch of VPPs [5].

## B. Research Gaps and Contributions

The literature review reveals the following research gaps:

- Prior studies show that decomposition methods effectively enhance the scalability of energy dispatch problems along the scenario and asset dimensions [10], [16]–[20], while TSA, particularly a posteriori TSA, has proven effective in reducing the temporal dimension without compromising solution accuracy [27]–[31]. However, the systematic integration of these two complementary methodologies within MPC schemes remains largely unexplored, leaving significant potential for further reducing the computational complexity of real-time controllers.
- Existing research on performance guarantees for TSA methods has primarily focused on establishing bounds on the approximation error incurred by aggregated optimization models relative to their full-scale counterparts. To date, such guarantees have been derived only for LP [35], MILP, and MIQP problems [36], typically by constructing aggregated models in which the decision variables are averaged over the representative time periods. However, for QCQP problems commonly encountered in VPP dispatch [5], the simultaneous presence of quadratic constraints, time-varying parameters, and intertemporal constraints (e.g., due to storage and ramping) renders this averaging approach insufficient: as discussed in Section II, the previously established bounds no longer hold.

This paper seeks to address these research gaps through the following **key contributions**:

- We formulate the energy dispatch of a VPP as a QCQP problem and propose a stochastic MPC scheme for its real-time solution. The stochastic MPC scheme is decomposed along both its asset and scenario dimensions using consensus ADMM, and temporally aggregated via TSA. This integrated approach, featuring a novel combination of MPC, TSA, and distributed optimization, simultaneously addresses all complexity dimensions of the dispatch problem, thereby maximizing computational efficiency.
- We demonstrate that the derived controller always provides a lower bound on the optimal objective function value of its full-scale counterpart, even in the presence of quadratic constraints, time-varying parameters, and intertemporal constraints such as storage and ramping.
- Leveraging the solution of the temporally aggregated and distributed controller, we propose an algorithm to systematically compute an upper bound on the optimal objective function value of the full-scale dispatch problem. The gap between the upper and lower bounds quantifies the approximation error incurred at each MPC iteration, thereby providing a rigorous performance guarantee.
- Although the derived bounds hold independently of the clustering technique employed for TSA, we show that incorporating dual information from the dispatch model into the clustering features yields a temporally aggregated controller that **exactly** reproduces the full-scale solution. Since such dual information is not available *ex ante*, we propose a closed-loop, a posteriori TSA method leveraging past MPC iterations to estimate it.

TABLE I  
COMPARISON OF THIS STUDY WITH THE RELEVANT RELATED LITERATURE

Ref.	MPC	Problem	Decomposition	Distributed method	TSA	Performance-guaranteed
[9]	✓(stochastic)	QP	×	—	×	✓
[11]	✓(chance-constrained)	QP	×	—	×	✓
[16]	✓(deterministic)	QP	Asset	Dual decomposition	×	✓
[10]	✓(robust)	MILP	Asset	ATC	×	×
[20]	✓(stochastic)	MIQP	Asset	ADMM	×	×
[18]	✓(stochastic)	QP	Scenario & temporal	OCD	×	✓
[29]	×	LP	×	—	✓(a priori)	×
[30]	×	MILP	×	—	✓(a posteriori)	×
[35]	×	LP	×	—	✓(a priori)	✓
[36]	×	MILP & MIQP	×	—	✓(a priori)	✓
[34]	✓(deterministic)	MIQP	×	—	✓(a priori)	×
This paper	✓(stochastic)	QCQP	Asset & scenario	ADMM	✓(a posteriori)	✓

Table I compares this study with the relevant related literature.

The remainder of the paper is organized as follows: Section II details the proposed methodology, Section III presents the results, and Section IV concludes the study.

## II. METHODOLOGY

In the following, sets and vectors are denoted in boldface (e.g.,  $\mathbf{z}$ ). The cardinality of a set is denoted by  $|\cdot|$ , while  $\|\cdot\|_2$  denotes the Euclidean ( $\ell_2$ ) norm. The maximum and minimum elements of a set  $\Phi$  are denoted by  $\max(\Phi)$  and  $\min(\Phi)$ , respectively. The zero vector is denoted by  $\mathbf{0}$ . All sets are indexed starting from 0.

### A. Overview of the Proposed Methodology

In this section, we present the proposed methodology for real-time VPP dispatch under uncertainty. The VPP comprises vRES, namely wind and solar, a set of energy storage systems  $\mathbf{N}$  indexed by  $n$ , and a set of thermal power plants  $\mathbf{G}$  indexed by  $g$ . The dispatch problem is subject to various uncertainties, namely vRES generation, energy demand, and energy prices, captured by a set of scenarios  $\Omega$  indexed by  $\omega$ . While vRES are non-dispatchable, storage and thermal units can be dispatched to maximize profit while meeting the VPP internal demand, with any imbalances accommodated via non-supplied energy. The VPP modeling is detailed in Subsection II-B.

The dispatch problem is addressed using a stochastic MPC scheme, as discussed in Subsection II-C. At each time step  $t \in \mathbf{T}$ , the MPC scheme is solved over a prediction horizon  $\mathbf{K}$ , indexed by  $k$ , with cardinality  $K := |\mathbf{K}|$  and sampling time  $\Delta$ . Following the standard MPC paradigm, at each time step  $t$ , only the first control action (corresponding to  $k = 0$ ) is applied, after which the horizon is advanced by one time step. To streamline the notation, we use the subscript  $k$  to denote variables and parameters associated with time  $t + k$ , i.e., the  $k$ -th prediction step of the MPC iteration executed at time  $t$ .

Our goal is to optimize the real-time energy dispatch of a VPP while simultaneously reducing the computational complexity of the problem across its asset, scenario, and temporal dimensions. To achieve this, we propose a novel integration of MPC, a posteriori TSA, and distributed optimization. Fig. 1 presents an overview of the proposed methodology.

The a posteriori TSA module exploits dual information from the previous MPC iteration to aggregate the full-scale

controller across  $\mathbf{R}$  representative time periods, indexed by  $r$ . The resulting temporally aggregated controller is then simultaneously decomposed across assets and scenarios, yielding the proposed **temporally aggregated and distributed stochastic MPC scheme**, as detailed in Subsection II-F. The temporally aggregated stochastic MPC scheme and a posteriori TSA method are detailed in Subsections II-D and II-E, respectively.

As illustrated in Fig. 1, the controller delivers a rigorous **performance guarantee** via iteratively refined upper and lower bounds on the full-scale optimal objective function value. The gap between these bounds enables the decision-maker to assess the controller performance without requiring the full-scale model solution, as discussed in Subsection II-G.

### B. Modeling

The VPP dispatch is modeled as follows. For each scenario  $\omega$  and time step  $k$ , the forecasts of vRES generation, demand, and energy prices are denoted by  $P_{\omega,k}^{\text{vRES}}$ ,  $D_{\omega,k}$ , and  $\pi_{\omega,k}$ , respectively. The energy output of the VPP in scenario  $\omega$  at time  $k$  is denoted by  $e_{\omega,k}$ , while  $e_{\omega,k}^{\text{ns}}$  is the non-supplied energy demand. For each storage unit  $n$ , the state of charge at time  $k$  in scenario  $\omega$  is denoted by  $e_{n,\omega,k}^s$ , with charging and discharging powers denoted by  $p_{n,\omega,k}^c$  and  $p_{n,\omega,k}^d$ , respectively. The minimum and maximum charging (discharging) power limits are denoted by  $\underline{P}_n^c$  and  $\overline{P}_n^c$  ( $\underline{P}_n^d$  and  $\overline{P}_n^d$ ). Charging and discharging efficiencies are denoted by  $\eta_n^c$  and  $\eta_n^d$ . The initial state of charge is  $E_n^{s,0}$ , while the lower and upper bounds on the state of charge are  $\underline{E}_n^s$  and  $\overline{E}_n^s$ , respectively.

The dynamics of each energy storage system are given by

$$e_{n,\omega,k+1}^s = e_{n,\omega,k}^s + (\eta_n^c p_{n,\omega,k}^c - \eta_n^d p_{n,\omega,k}^d) \Delta, \quad \forall n, \forall \omega, \forall k \in \mathbf{K} \setminus \{K-1\}, \quad (1)$$

$$e_{n,\omega,0}^s = E_n^{s,0}, \quad \forall n, \forall \omega, \quad (2)$$

$$\underline{E}_n^s \leq e_{n,\omega,k}^s \leq \overline{E}_n^s, \quad \forall n, \forall \omega, \forall k. \quad (3)$$

The charging and discharging powers are constrained by

$$\underline{P}_n^c \leq p_{n,\omega,k}^c \leq \overline{P}_n^c, \quad \forall n, \forall \omega, \forall k, \quad (4)$$

$$\underline{P}_n^d \leq p_{n,\omega,k}^d \leq \overline{P}_n^d, \quad \forall n, \forall \omega, \forall k. \quad (5)$$

The power output of each thermal unit  $g$ , denoted  $p_{g,\omega,k}^{\text{th}}$ , is constrained between its lower ( $\underline{P}_g^{\text{th}}$ ) and upper ( $\overline{P}_g^{\text{th}}$ ) limits as

$$\underline{P}_g^{\text{th}} \leq p_{g,\omega,k}^{\text{th}} \leq \overline{P}_g^{\text{th}}, \quad \forall g, \forall \omega, \forall k. \quad (6)$$

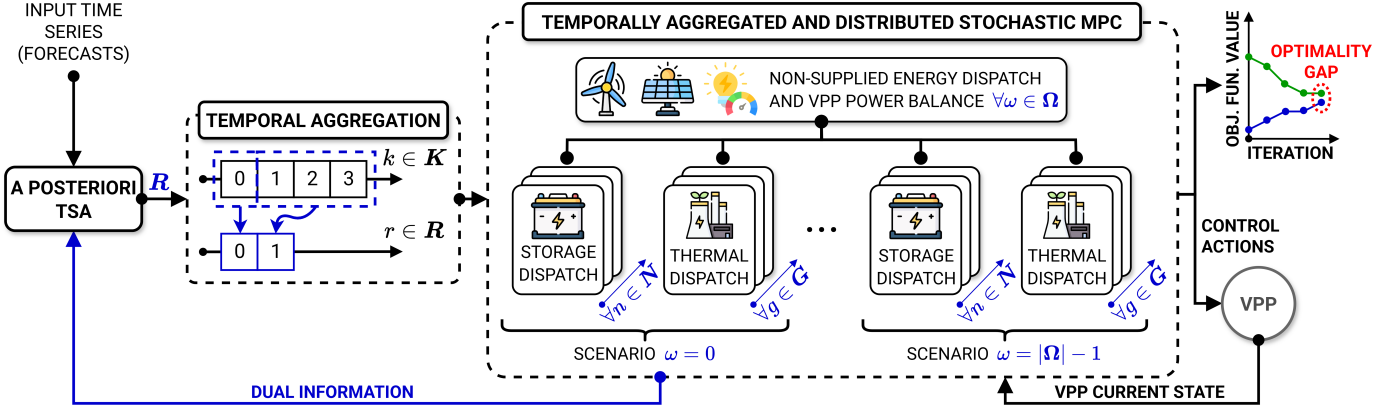


Fig. 1. Illustration of the proposed methodology for real-time energy dispatch of a VPP under uncertainty.

Moreover, the thermal power generation of the VPP is subject to the following quadratic emission constraints [37]:

$$\alpha_g (p_{g,\omega,k}^{\text{th}})^2 + \beta_g p_{g,\omega,k}^{\text{th}} \leq L_g^{\text{CO}_2}, \quad \forall g, \forall \omega, \forall k, \quad (7)$$

where  $L_g^{\text{CO}_2}$  is the emission limit of generator  $g$ , while  $\alpha_g$  and  $\beta_g$  are the coefficients mapping its output to emissions.

Each thermal unit is subject to its ramp limit  $R_g^{\text{th}}$  as

$$p_{g,\omega,k+1}^{\text{th}} - p_{g,\omega,k}^{\text{th}} \leq R_g^{\text{th}}, \quad \forall g, \forall \omega, \forall k \in \mathbf{K} \setminus \{K-1\}, \quad (8)$$

$$p_{g,\omega,k}^{\text{th}} - p_{g,\omega,k+1}^{\text{th}} \leq R_g^{\text{th}}, \quad \forall g, \forall \omega, \forall k \in \mathbf{K} \setminus \{K-1\}. \quad (9)$$

### C. Full-Scale Controller

We formulate the VPP energy dispatch as a stochastic MPC problem. Let  $\mathbf{u}_0$  denote the vector of decision variables computed for  $k=0$ . We define the set of decision variables as  $\mathbf{z} := \{\mathbf{u}_0, e_{\omega,k}, e_{\omega,k}^{\text{ns}}, e_{n,\omega,k}^s, p_{g,\omega,k}^{\text{th}}, p_{n,\omega,k}^c, p_{n,\omega,k}^d\}_{n \in \mathbf{N}, g \in \mathbf{G}, \omega \in \Omega, k \in \mathbf{K}}$ .

Let  $C_n^c$  and  $C_n^d$  denote the charging and discharging costs of storage unit  $n$ , respectively, and let  $C_g^{\text{th}}$  represent the generation cost of thermal unit  $g$ . The penalty associated with non-supplied energy is denoted by  $C^{\text{ns}}$ . Furthermore, a reference state  $E_n^{\text{ref}}$  is specified for each storage unit  $n$ ; deviations from this reference are penalized by  $C_n^{\text{ref}}$ .

The goal is to minimize the objective function

$$\begin{aligned} F(\mathbf{z}) := & \sum_{\omega \in \Omega} \sum_{k \in \mathbf{K}} \left( -\pi_{\omega,k} e_{\omega,k} + \sum_{g \in \mathbf{G}} C_g^{\text{th}} p_{g,\omega,k}^{\text{th}} \Delta + C^{\text{ns}} e_{\omega,k} \right. \\ & \left. + \sum_{n \in \mathbf{N}} (C_n^c p_{n,\omega,k}^c + C_n^d p_{n,\omega,k}^d) \Delta \right) \\ & + \sum_{n \in \mathbf{N}} \sum_{\omega \in \Omega} \sum_{k \in \mathbf{K}} C_n^{\text{ref}} (e_{n,\omega,k}^s - E_n^{\text{ref}})^2. \end{aligned} \quad (10)$$

In (10), linear terms capture the VPP profit, while the quadratic term penalizes storage deviations from the reference states.

At each time  $t \in \mathbf{T}$ , the **full-scale stochastic MPC scheme** solves the following QCQP problem over the horizon  $\mathbf{K}$ :

$$\begin{aligned} \min_{\mathbf{z}} \quad & F(\mathbf{z}) \\ \text{s.t.} \quad & e_{\omega,k} = P_{\omega,k}^{\text{vRES}} \Delta - D_{\omega,k} + \sum_{n \in \mathbf{N}} (p_{n,\omega,k}^d - p_{n,\omega,k}^c) \Delta \end{aligned} \quad (11a)$$

$$+ \sum_{g \in \mathbf{G}} p_{g,\omega,k}^{\text{th}} \Delta + e_{\omega,k}^{\text{ns}}, \quad \forall \omega, \forall k, \quad (11b)$$

$$(1) - (9),$$

$$[e_{\omega,0}^{\text{ns}}, p_{g,\omega,0}^{\text{th}}, p_{n,\omega,0}^c, p_{n,\omega,0}^d] = \mathbf{u}_0, \quad \forall n, \forall g, \forall \omega, \quad (11c)$$

$$\mathbf{z} \geq \mathbf{0}. \quad (11d)$$

In (11), the constraints (11b) enforce the energy balance within the VPP, while (11c) are the non-anticipativity constraints.

### D. Temporally Aggregated Controller

To alleviate computational burden, we employ TSA to construct a temporally aggregated counterpart of (11), defined over  $\mathbf{R}$  representative time periods, with  $R := |\mathbf{R}|$ . When  $R \ll K$ , solving the aggregated model in place of its full-scale counterpart yields a significant computational advantage.

Let  $\mathbf{K}_r \subseteq \mathbf{K}$  denote the set of time periods assigned to cluster  $r \in \mathbf{R}$ , with cardinality  $K_r := |\mathbf{K}_r|$ . We collect the decision variables of the aggregated model in  $\bar{\mathbf{z}} := \{\bar{\mathbf{u}}_0, \bar{e}_{\omega,r}, \bar{e}_{\omega,r}^{\text{ns}}, \bar{e}_{n,\omega,r}^s, \bar{p}_{g,\omega,r}^{\text{th}}, \bar{p}_{n,\omega,r}^c, \bar{p}_{n,\omega,r}^d\}_{n \in \mathbf{N}, g \in \mathbf{G}, \omega \in \Omega, r \in \mathbf{R}}$ .

We define the aggregated counterpart of  $F(\mathbf{z})$  in (10) as

$$\begin{aligned} \bar{F}(\bar{\mathbf{z}}) := & \sum_{\omega \in \Omega} \sum_{r \in \mathbf{R}} K_r \left( -\max_{k \in \mathbf{K}_r} \{\pi_{\omega,k}\} \bar{e}_{\omega,r} + \sum_{g \in \mathbf{G}} C_g^{\text{th}} \bar{p}_{g,\omega,r}^{\text{th}} \Delta \right. \\ & \left. + C^{\text{ns}} \bar{e}_{\omega,r} + \sum_{n \in \mathbf{N}} (C_n^c \bar{p}_{n,\omega,r}^c + C_n^d \bar{p}_{n,\omega,r}^d) \Delta \right) \\ & + \sum_{n \in \mathbf{N}} \sum_{\omega \in \Omega} \sum_{r \in \mathbf{R}} C_n^{\text{ref}} (\bar{e}_{n,\omega,r}^s - E_n^{\text{ref}})^2. \end{aligned} \quad (12)$$

At each time  $t \in \mathbf{T}$ , the **temporally aggregated stochastic MPC scheme** solves the following QCQP problem over  $\mathbf{R}$ :

$$\min_{\bar{\mathbf{z}}} \quad \bar{F}(\bar{\mathbf{z}}) \quad (13a)$$

$$\begin{aligned} \text{s.t.} \quad & \bar{e}_{\omega,r} = \sum_{k \in \mathbf{K}_r} \frac{P_{\omega,k}^{\text{vRES}} \Delta - D_{\omega,k}}{K_r} + \sum_{g \in \mathbf{G}} \bar{p}_{g,\omega,r}^{\text{th}} \Delta + \bar{e}_{\omega,r}^{\text{ns}} \\ & + \sum_{n \in \mathbf{N}} (\bar{p}_{n,\omega,r}^d - \bar{p}_{n,\omega,r}^c) \Delta, \quad \forall \omega, \forall r, \end{aligned} \quad (13b)$$

$$\begin{aligned} \bar{e}_{n,\omega,r+1}^s = & \bar{e}_{n,\omega,r}^s + K_r (\eta_n^c \bar{p}_{n,\omega,r}^c - \eta_n^d \bar{p}_{n,\omega,r}^d) \Delta, \\ & \forall n, \forall \omega, \forall r \in \mathbf{R} \setminus \{R-1\}, \end{aligned} \quad (13c)$$

$$\bar{e}_{n,\omega,0}^s = E_n^{s,0}, \quad \forall n, \forall \omega, \quad (13d)$$

$$\underline{E}_n^s \leq \bar{e}_{n,\omega,r}^s \leq \bar{E}_n^s, \quad \forall n, \forall \omega, \forall r, \quad (13e)$$

$$\underline{P}_n^c \leq \bar{p}_{n,\omega,r}^c \leq \bar{P}_n^c, \quad \forall n, \forall \omega, \forall r, \quad (13f)$$

$$\underline{P}_n^d \leq \bar{p}_{n,\omega,r}^d \leq \bar{P}_n^d, \quad \forall n, \forall \omega, \forall r, \quad (13g)$$

$$\underline{P}_g^{\text{th}} \leq \bar{p}_{g,\omega,r}^{\text{th}} \leq \bar{P}_g^{\text{th}}, \quad \forall g, \forall \omega, \forall r, \quad (13h)$$

$$\alpha_g K_r (\bar{p}_{g,\omega,r}^{\text{th}})^2 - \alpha_g (K_r - 1) (\bar{P}_g^{\text{th}})^2 + \beta_g \bar{p}_{g,\omega,r}^{\text{th}} \leq L_g^{\text{CO}_2}, \quad \forall g, \forall \omega, \forall r, \quad (13i)$$

$$\bar{p}_{g,\omega,r+1}^{\text{th}} - \bar{p}_{g,\omega,r}^{\text{th}} K_r \leq R_g^{\text{th}} + R_g^{\text{th}} \frac{K_{r+1} - 1}{2}, \quad \forall g, \forall \omega, \forall r \in \mathbf{R} \setminus \{R-1\}, \quad (13j)$$

$$\bar{p}_{g,\omega,r}^{\text{th}} - \bar{p}_{g,\omega,r+1}^{\text{th}} K_{r+1} \leq R_g^{\text{th}} + R_g^{\text{th}} \frac{K_r - 1}{2}, \quad \forall g, \forall \omega, \forall r \in \mathbf{R} \setminus \{R-1\}, \quad (13k)$$

$$[\bar{e}_{\omega,0}^{\text{ns}}, \bar{p}_{g,\omega,0}^{\text{th}}, \bar{p}_{n,\omega,0}^c, \bar{p}_{n,\omega,0}^d] = \bar{\mathbf{u}}_0, \quad \forall n, \forall g, \forall \omega, \quad (13l)$$

$$\bar{\mathbf{z}} \geq \mathbf{0}. \quad (13m)$$

Here, (13b), (13c)–(13k), (13l), and (13m) are the aggregated counterparts of (11b), (1)–(9), (11c), and (11d), respectively.

Notably, whereas conventional TSA methods average the input time series over each cluster [26], we introduce a novel formulation that instead considers the cluster-wise maximum price in (12) and augments the quadratic constraints (13i) and the intertemporal constraints (13c), (13j), and (13k) with cluster-specific terms. This ensures that the temporally aggregated model (13) inherently satisfies the desired theoretical properties, as formally established in Subsection II-G.

### E. Closed-Loop A Posteriori Time Series Aggregation

Once the temporally aggregated model (13) is constructed, a clustering technique is required to extract representative time periods from the original prediction horizon  $\mathbf{K}$ . Owing to the presence of intertemporal constraints in (11), conventional clustering techniques (e.g., k-means) cannot be directly employed, as they disregard temporal chronology. To address this issue, we employ a *sliding window clustering* technique.

Let  $\{\mathbf{a}_k\}_{k \in \mathbf{K}}$  be the set of clustering features used for TSA. This technique evaluates the similarity between consecutive elements of  $\{\mathbf{a}_k\}$ , assigning  $k$  to the current cluster  $r$  if

$$\|\mathbf{a}_k - \boldsymbol{\mu}_r\|_2 \leq \zeta, \quad (14)$$

where  $\zeta$  is a user-defined similarity threshold and  $\boldsymbol{\mu}_r$  denotes the centroid of cluster  $r$ , computed as  $\boldsymbol{\mu}_r := \frac{1}{K_r} \sum_{k \in \mathbf{K}_r} \mathbf{a}_k$ . If condition (14) is not satisfied for  $\mathbf{a}_k$ , the current cluster is closed and a new cluster is initialized starting at  $k$ .

Fig. 2 illustrates the sliding window clustering technique. Starting from an initial cluster (e.g., containing  $k-1$  and  $k$ ), the cluster is extended to include  $k+1$  only if condition (14) is satisfied for  $\mathbf{a}_{k+1}$ , thereby ensuring temporal coherence.

The features used for TSA directly affect the fidelity of the aggregated model. In particular, [31] demonstrates that if the active constraints of the full-scale model were known, an aggregated model could be constructed that exactly reproduces the optimal objective function value of the full-scale model.

Although such information is unavailable *ex ante*, MPC offers a unique opportunity to exploit it retrospectively, as

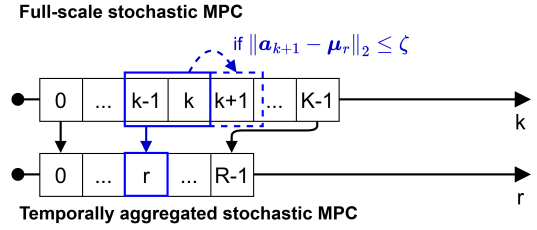


Fig. 2. Illustration of the sliding window clustering technique.

the same optimization problem is repeatedly solved over overlapping horizons, differing only by the newly appended terminal time step and the set of scenarios considered at each MPC iteration. Consequently, the outputs from previous MPC runs can inform TSA in a closed-loop manner.

Motivated by this insight, we propose a closed-loop a posteriori TSA method integrated with MPC. At each iteration  $t$ , the dual information from the MPC problem solved at time  $t-1$  is used as a feature in the sliding window clustering technique to identify the representative periods  $\mathbf{R}$  (see Fig. 1). Specifically, we use estimates of the marginal costs, i.e., the dual variables associated with the energy balance constraints (11b), which, as shown in Section III, serve as an accurate proxy for identifying the active constraints of (11). Two singleton clusters are enforced at the first and last time steps of  $\mathbf{K}$ , reflecting the absence of dual information at the terminal step and the critical role of the initial step, whose control actions are implemented at time  $t$ . By exploiting dual information from the previous MPC iteration, our method estimates the active constraints of (11), directly targeting exact temporal aggregation, which is typically unattainable with traditional a priori TSA methods.

### F. Temporally Aggregated and Distributed Controller

To further reduce the computational complexity arising from the asset and scenario dimensions, we decompose the temporally aggregated model (13) via consensus ADMM [21].

The aggregated model (13) features three sets of coupling constraints: intertemporal coupling induced by the storage (13c) and ramping constraints (13j)–(13k), asset coupling arising from the energy balance constraints (13b), and scenario coupling induced by the non-anticipativity constraints (13l). All coupling constraints in (13) involve three sets of *global variables*:  $\bar{\mathbf{p}}_{n,\omega}^c := [\bar{p}_{n,\omega,0}^c, \dots, \bar{p}_{n,\omega,r}^c, \dots, \bar{p}_{n,\omega,R-1}^c]^\top$ ,  $\bar{\mathbf{p}}_{n,\omega}^d := [\bar{p}_{n,\omega,0}^d, \dots, \bar{p}_{n,\omega,r}^d, \dots, \bar{p}_{n,\omega,R-1}^d]^\top$ , and  $\bar{\mathbf{p}}_{g,\omega}^{\text{th}} := [\bar{p}_{g,\omega,0}^{\text{th}}, \dots, \bar{p}_{g,\omega,r}^{\text{th}}, \dots, \bar{p}_{g,\omega,R-1}^{\text{th}}]^\top$ . We relax the coupling constraints in (13) by introducing copies of these global variables.

Let  $\{\hat{\mathbf{p}}_{n,\omega}^c, \hat{\mathbf{p}}_{n,\omega}^d, \hat{\mathbf{p}}_{g,\omega}^{\text{th}}\}$  and  $\{\tilde{\mathbf{p}}_{n,\omega}^c, \tilde{\mathbf{p}}_{n,\omega}^d, \tilde{\mathbf{p}}_{g,\omega}^{\text{th}}\}$  denote two distinct sets of copies of the global variables in (13). By introducing these copies, we reformulate the temporally aggregated model (13) as the following consensus problem:

$$\min_{\bar{\mathbf{z}}} \bar{F}(\bar{\mathbf{z}}) \quad (15a)$$

$$\text{s.t. } \mathbf{z}^b \in \Xi(\boldsymbol{\beta}), \quad (15b)$$

$$\mathbf{z}_{n,\omega}^s \in \Gamma_{n,\omega}^s(\boldsymbol{\theta}_{n,\omega}^s), \quad \forall n, \forall \omega, \quad (15c)$$

$$\tilde{\mathbf{p}}_{g,\omega}^{\text{th}} \in \Gamma_{g,\omega}^{\text{th}}(\boldsymbol{\theta}_{g,\omega}^{\text{th}}), \quad \forall g, \forall \omega, \quad (15d)$$

$$\bar{\mathbf{p}}_{n,\omega}^s = \hat{\mathbf{p}}_{n,\omega}^s : \hat{\lambda}_{n,\omega}^s, \forall n, \forall \omega, \quad (15e)$$

$$\bar{\mathbf{p}}_{n,\omega}^s = \tilde{\mathbf{p}}_{n,\omega}^s : \tilde{\lambda}_{n,\omega}^s, \forall n, \forall \omega, \quad (15f)$$

$$\bar{\mathbf{p}}_{g,\omega}^{\text{th}} = \hat{\mathbf{p}}_{g,\omega}^{\text{th}} : \hat{\lambda}_{g,\omega}^{\text{th}}, \forall g, \forall \omega, \quad (15g)$$

$$\bar{\mathbf{p}}_{g,\omega}^{\text{th}} = \tilde{\mathbf{p}}_{g,\omega}^{\text{th}} : \tilde{\lambda}_{g,\omega}^{\text{th}}, \forall g, \forall \omega, \quad (15h)$$

where  $\hat{\lambda}_{n,\omega}^s := [\hat{\lambda}_{n,\omega}^c, \hat{\lambda}_{n,\omega}^d]^\top$ ,  $\tilde{\lambda}_{n,\omega}^s := [\tilde{\lambda}_{n,\omega}^c, \tilde{\lambda}_{n,\omega}^d]^\top$ ,  $\tilde{\mathbf{p}}_{n,\omega}^s := [\tilde{\mathbf{p}}_{n,\omega}^c, \tilde{\mathbf{p}}_{n,\omega}^d]^\top$ ,  $\hat{\mathbf{p}}_{n,\omega}^s := [\hat{\mathbf{p}}_{n,\omega}^c, \hat{\mathbf{p}}_{n,\omega}^d]^\top$ ,  $\bar{\mathbf{p}}_{n,\omega}^s := [\bar{\mathbf{p}}_{n,\omega}^c, \bar{\mathbf{p}}_{n,\omega}^d]^\top$ ,  $\mathbf{z}^b := \{\bar{\mathbf{u}}_0, \bar{\mathbf{e}}_{\omega,r}, \bar{\mathbf{e}}_{\omega,r}^{\text{ns}}, \hat{\mathbf{p}}_{n,\omega}^c, \hat{\mathbf{p}}_{n,\omega}^d, \hat{\mathbf{p}}_{g,\omega}^{\text{th}}\}_{n \in \mathcal{N}, g \in \mathcal{G}, \omega \in \Omega, r \in \mathcal{R}}$  and  $\mathbf{z}_{n,\omega}^s := \{\bar{\mathbf{e}}_{n,\omega}^s, \bar{\mathbf{p}}_{n,\omega}^c, \bar{\mathbf{p}}_{n,\omega}^d\}$ .

This reformulation introduces three sets of temporally aggregated subproblems:

- Subproblem (16), corresponding to (15b), with local variables  $\mathbf{z}^b$ , and feasible set  $\Xi(\beta)$ , defined by (13b), (13f)–(13h), (13l) and (13m), with parameters  $\beta$ .
- $|\mathcal{N}| \times |\Omega|$  subproblems (17), corresponding to (15c), with local variables  $\mathbf{z}_{n,\omega}^s$ , and feasible set  $\Gamma_{n,\omega}^s (\theta_{n,\omega}^s)$ , defined by (13c)–(13g) and (13m), with parameters  $\theta_{n,\omega}^s$ .
- $|\mathcal{G}| \times |\Omega|$  subproblems (18), corresponding to (15d), with local variables  $\bar{\mathbf{p}}_{g,\omega}^{\text{th}}$  and feasible set  $\Gamma_{g,\omega}^{\text{th}} (\theta_{g,\omega}^{\text{th}})$  defined by (13h)–(13k) and (13m), with parameters  $\theta_{g,\omega}^{\text{th}}$ .

Consistency among the local variables is enforced by the consensus constraints (15e)–(15h), with associated dual variables  $\hat{\lambda}_{n,\omega}^s$ ,  $\tilde{\lambda}_{n,\omega}^s$ ,  $\hat{\lambda}_{g,\omega}^{\text{th}}$ , and  $\tilde{\lambda}_{g,\omega}^{\text{th}}$ . Separately for each scenario, the subproblems (17) and (18) determine the dispatch of each storage and thermal unit, respectively, while (16) enforces the VPP energy balance. The derived  $(|\mathcal{N}| + |\mathcal{G}|) \times |\Omega| + 1$  subproblems are solved **in parallel** via consensus ADMM.

Let  $\rho$  be ADMM step size. At time  $t$ , our **temporally aggregated and distributed stochastic MPC scheme** executes the following steps over  $i \in \mathcal{I}$  iterations, with  $\mathcal{I} := |\mathcal{I}|$ .

**Step I.** Local primal variable update:

$$\begin{aligned} \mathbf{z}^{b^{i+1}} := \operatorname{argmin}_{\mathbf{z}^b \in \Xi} & \left\{ \sum_{\omega \in \Omega} \sum_{r \in \mathcal{R}} K_r \left( C^{\text{ns}} \bar{\mathbf{e}}_{\omega,r}^{\text{ns}} - \max_{k \in \mathcal{K}_r} \{\pi_{\omega,k}\} \bar{\mathbf{e}}_{\omega,r} \right) \right. \\ & + \sum_{n \in \mathcal{N}} \sum_{\omega \in \Omega} \left( \left( \hat{\lambda}_{n,\omega}^{s^i} \right)^\top \hat{\mathbf{p}}_{n,\omega}^s + \frac{\rho}{2} \left\| \hat{\mathbf{p}}_{n,\omega}^s - \bar{\mathbf{p}}_{n,\omega}^s \right\|_2^2 \right) \\ & \left. + \sum_{g \in \mathcal{G}} \sum_{\omega \in \Omega} \left( \left( \hat{\lambda}_{g,\omega}^{\text{th}^i} \right)^\top \hat{\mathbf{p}}_{g,\omega}^{\text{th}} + \frac{\rho}{2} \left\| \hat{\mathbf{p}}_{g,\omega}^{\text{th}} - \bar{\mathbf{p}}_{g,\omega}^{\text{th}} \right\|_2^2 \right) \right\}, \quad (16) \end{aligned}$$

$$\begin{aligned} \mathbf{z}_{n,\omega}^{s^{i+1}} := \operatorname{argmin}_{\mathbf{z}_{n,\omega}^s \in \Gamma_{n,\omega}^s} & \left\{ \sum_{n \in \mathcal{N}} \sum_{\omega \in \Omega} \sum_{r \in \mathcal{R}} \left( C_n^c \bar{\mathbf{p}}_{n,\omega,r}^c + C_n^d \bar{\mathbf{p}}_{n,\omega,r}^d \right) K_r \Delta \right. \\ & + \sum_{n \in \mathcal{N}} \sum_{\omega \in \Omega} \left( \sum_{r \in \mathcal{R}} C_n^{\text{ref}} \left( \bar{\mathbf{e}}_{n,\omega,r}^s - E_n^{\text{ref}} \right)^2 + \left( \tilde{\lambda}_{n,\omega}^{s^i} \right)^\top \bar{\mathbf{p}}_{n,\omega}^s \right) \\ & \left. + \sum_{n \in \mathcal{N}} \sum_{\omega \in \Omega} \left( \frac{\rho}{2} \left\| \bar{\mathbf{p}}_{n,\omega}^s - \hat{\mathbf{p}}_{n,\omega}^s \right\|_2^2 \right) \right\}, \quad \forall n, \forall \omega, \quad (17) \end{aligned}$$

$$\begin{aligned} \bar{\mathbf{p}}_{g,\omega}^{\text{th}^{i+1}} := \operatorname{argmin}_{\bar{\mathbf{p}}_{g,\omega}^{\text{th}} \in \Gamma_{g,\omega}^{\text{th}}} & \left\{ \sum_{g \in \mathcal{G}} \sum_{\omega \in \Omega} \left( \sum_{r \in \mathcal{R}} C_g^{\text{th}} \bar{\mathbf{p}}_{g,\omega,r}^{\text{th}} K_r \Delta + \left( \tilde{\lambda}_{g,\omega}^{\text{th}^i} \right)^\top \bar{\mathbf{p}}_{g,\omega}^{\text{th}} \right) \right. \\ & \left. + \sum_{g \in \mathcal{G}} \sum_{\omega \in \Omega} \left( \frac{\rho}{2} \left\| \bar{\mathbf{p}}_{g,\omega}^{\text{th}} - \hat{\mathbf{p}}_{g,\omega}^{\text{th}} \right\|_2^2 \right) \right\}, \quad \forall g, \forall \omega. \quad (18) \end{aligned}$$

**Step II.** Global primal variable update:

$$\bar{\mathbf{p}}_{n,\omega}^{s^{i+1}} := \frac{1}{2} \left( \hat{\mathbf{p}}_{n,\omega}^{s^{i+1}} + \tilde{\mathbf{p}}_{n,\omega}^{s^{i+1}} \right), \quad \forall n, \forall \omega, \quad (19)$$

$$\bar{\mathbf{p}}_{g,\omega}^{\text{th}^{i+1}} := \frac{1}{2} \left( \hat{\mathbf{p}}_{g,\omega}^{\text{th}^{i+1}} + \tilde{\mathbf{p}}_{g,\omega}^{\text{th}^{i+1}} \right), \quad \forall g, \forall \omega. \quad (20)$$

**Step III.** Dual variable update:

$$\hat{\lambda}_{n,\omega}^{s^{i+1}} := \hat{\lambda}_{n,\omega}^{s^i} + \rho \left( \hat{\mathbf{p}}_{n,\omega}^{s^{i+1}} - \bar{\mathbf{p}}_{n,\omega}^{s^{i+1}} \right), \quad \forall n, \forall \omega, \quad (21)$$

$$\tilde{\lambda}_{n,\omega}^{s^{i+1}} := \tilde{\lambda}_{n,\omega}^{s^i} + \rho \left( \tilde{\mathbf{p}}_{n,\omega}^{s^{i+1}} - \bar{\mathbf{p}}_{n,\omega}^{s^{i+1}} \right), \quad \forall n, \forall \omega, \quad (22)$$

$$\hat{\lambda}_{g,\omega}^{\text{th}^{i+1}} := \hat{\lambda}_{g,\omega}^{\text{th}^i} + \rho \left( \hat{\mathbf{p}}_{g,\omega}^{\text{th}^{i+1}} - \bar{\mathbf{p}}_{g,\omega}^{\text{th}^{i+1}} \right), \quad \forall g, \forall \omega, \quad (23)$$

$$\tilde{\lambda}_{g,\omega}^{\text{th}^{i+1}} := \tilde{\lambda}_{g,\omega}^{\text{th}^i} + \rho \left( \tilde{\mathbf{p}}_{g,\omega}^{\text{th}^{i+1}} - \bar{\mathbf{p}}_{g,\omega}^{\text{th}^{i+1}} \right), \quad \forall g, \forall \omega. \quad (24)$$

To enhance convergence, we adopt the residual-based update rule for  $\rho$ , initialized at  $\rho^0$ , as proposed in [21].

### G. Derivation of the Objective Function Bounds

In Subsection II-F, the aggregated model (13) is decomposed using ADMM. Since (13) is convex, ADMM is guaranteed to converge to its optimal objective function value [21]. However, (13) is an approximation of the original full-scale model (11). To establish a formal performance guarantee, we bound the resulting approximation error as follows.

**Proposition 1.** *Let  $\mathbf{z}$  be a feasible solution to the full-scale model (11). Let  $\bar{\mathbf{z}}$  be derived from  $\mathbf{z}$  as*

$$\bar{\mathbf{e}}_{\omega,r} := \sum_{k \in \mathcal{K}_r} \frac{e_{\omega,k}}{K_r}, \quad (25) \quad \bar{\mathbf{e}}_{\omega,r}^{\text{ns}} := \sum_{k \in \mathcal{K}_r} \frac{e_{\omega,k}^{\text{ns}}}{K_r}, \quad (26)$$

$$\bar{\mathbf{e}}_{n,\omega,r}^s := e_{n,\omega,\min(\mathcal{K}_r)}, \quad (27) \quad \bar{\mathbf{p}}_{g,\omega,r}^{\text{th}} := \sum_{k \in \mathcal{K}_r} \frac{p_{g,\omega,k}^{\text{th}}}{K_r}, \quad (28)$$

$$\bar{\mathbf{p}}_{n,\omega,r}^c := \sum_{k \in \mathcal{K}_r} \frac{p_{n,\omega,k}^c}{K_r}, \quad (29) \quad \bar{\mathbf{p}}_{n,\omega,r}^d := \sum_{k \in \mathcal{K}_r} \frac{p_{n,\omega,k}^d}{K_r}, \quad (30)$$

$\forall n, \forall g, \forall \omega, \forall r$ . Then,  $\bar{\mathbf{z}}$  is a feasible solution to the temporally aggregated model (13) and it holds that  $\bar{F}(\bar{\mathbf{z}}) \leq F(\mathbf{z})$ .

*Proof.* We first demonstrate that any  $\bar{\mathbf{z}}$  obtained through (25)–(30) is feasible for the temporally aggregated model (13).

Using (30), we reformulate (13j) and (13k) as

$$\begin{aligned} \bar{\mathbf{p}}_{g,\omega,r+1}^{\text{th}} - \bar{\mathbf{p}}_{g,\omega,r}^{\text{th}} K_r &= \sum_{k \in \mathcal{K}_{r+1}} \frac{p_{g,\omega,k}^{\text{th}}}{K_{r+1}} - \sum_{k \in \mathcal{K}_r} p_{g,\omega,k}^{\text{th}} \\ &\leq p_{g,\omega,\min(\mathcal{K}_{r+1})}^{\text{th}} + R_g^{\text{th}} \frac{K_{r+1} - 1}{2} - p_{g,\omega,\max(\mathcal{K}_r)}^{\text{th}} \\ &\leq R_g^{\text{th}} + R_g^{\text{th}} \frac{K_{r+1} - 1}{2}, \quad \forall g, \forall \omega, \forall r \in \mathcal{R} \setminus \{R-1\}, \quad (31) \end{aligned}$$

and

$$\begin{aligned} \bar{\mathbf{p}}_{g,\omega,r}^{\text{th}} - \bar{\mathbf{p}}_{g,\omega,r+1}^{\text{th}} K_{r+1} &= \sum_{k \in \mathcal{K}_r} \frac{p_{g,\omega,k}^{\text{th}}}{K_r} - \sum_{k \in \mathcal{K}_{r+1}} p_{g,\omega,k}^{\text{th}} \\ &\leq p_{g,\omega,\max(\mathcal{K}_r)}^{\text{th}} + R_g^{\text{th}} \frac{K_r - 1}{2} - p_{g,\omega,\min(\mathcal{K}_{r+1})}^{\text{th}} \\ &\leq R_g^{\text{th}} + R_g^{\text{th}} \frac{K_r - 1}{2}, \quad \forall g, \forall \omega, \forall r \in \mathcal{R} \setminus \{R-1\}, \quad (32) \end{aligned}$$

respectively.

Using (28), we reformulate (13i) as

$$\begin{aligned} & \frac{\alpha_g}{K_r} \left( \sum_{k \in \mathbf{K}_r} p_{g,\omega,k}^{\text{th}} \right)^2 - \alpha_g (K_r - 1) \left( \bar{P}_g^{\text{th}} \right)^2 + \frac{\beta_g}{K_r} \sum_{k \in \mathbf{K}_r} p_{g,\omega,k}^{\text{th}} \\ & \leq \sum_{k \in \mathbf{K}_r} \frac{\alpha_g \left( p_{g,\omega,k}^{\text{th}} \right)^2 + \beta_g p_{g,\omega,k}^{\text{th}}}{K_r} \leq L_g^{\text{CO}_2}, \quad \forall g, \forall \omega, \forall r. \end{aligned} \quad (33)$$

The full-scale constraints (8), (9), and (7) imply the aggregated constraints (31), (32), and (33), respectively, since they are enforced over the set  $\mathbf{K}_r$  rather than over the individual time steps  $k$ . Similarly, constraints (11b), (1)–(6), and (11c) imply (13b)–(13h) and (13l), as demonstrated in [36]. It follows that any  $\bar{\mathbf{z}}$  obtained from a feasible solution  $\mathbf{z}$  of the full-scale model (11) via (25)–(30) is feasible for (13).

Finally, substituting  $\bar{\mathbf{z}}$  into  $\bar{F}(\bar{\mathbf{z}})$ , as defined in (12), yields

$$\begin{aligned} & \sum_{\omega \in \Omega} \sum_{r \in \mathbf{R}} \left( - \max_{k \in \mathbf{K}_r} \{ \pi_{\omega,k} \} \sum_{k \in \mathbf{K}_r} e_{\omega,k} \right) + \sum_{\omega \in \Omega} \sum_{k \in \mathbf{K}} C_n^{\text{ns}} e_{\omega,k}^{\text{ns}} \\ & + \sum_{\omega \in \Omega} \sum_{k \in \mathbf{K}} \left( \sum_{g \in \mathbf{G}} C_g^{\text{th}} p_{g,\omega,k}^{\text{th}} + \sum_{n \in \mathbf{N}} (C_n^{\text{c}} p_{n,\omega,k}^{\text{c}} + C_n^{\text{d}} p_{n,\omega,k}^{\text{d}}) \right) \Delta \\ & + \sum_{n \in \mathbf{N}} \sum_{\omega \in \Omega} \sum_{r \in \mathbf{R}} C_n^{\text{ref}} \left( e_{n,\omega,\min(\mathbf{K}_r)}^{\text{s}} - E_n^{\text{ref}} \right)^2 \leq F(\mathbf{z}), \end{aligned}$$

where  $F(\mathbf{z})$  is defined as in (10).  $\square$

In words, Proposition 1 asserts that every feasible solution of the full-scale model (11) corresponds to a feasible solution of the temporally aggregated model (13) with an equal or lower objective function value. Consequently, the controller proposed in Subsection II-F provides a guaranteed lower bound on the optimal objective function value of the original full-scale controller in Subsection II-C at each MPC iteration.

Once a lower bound  $F^{\text{LB}}$  on the full-scale optimal objective function value  $F^*$  is obtained, as established in Proposition 1, an upper bound  $F^{\text{UB}}$  is computed by solving (11) with the first-stage decisions  $\mathbf{u}_0$  fixed to those obtained from solving (13). Under this restriction, (11) can be solved in parallel across scenarios. The resulting **performance-guaranteed temporally aggregated and distributed stochastic MPC scheme** executes Algorithm 1 at each time step  $t \in \mathbf{T}$ .

Algorithm 1 is structured into a higher and a lower layer, executing  $j \in J$  and  $i \in I$  iterations, respectively. At time  $t$ , the **higher layer** receives the dual variable values computed at time  $t - 1$ , specifically the marginal cost estimates, which serve as features for the sliding window clustering technique detailed in Subsection II-E. The identified clusters are then used to construct the temporally aggregated model (13), which is passed to the **lower layer**. Here, the problem is decomposed into  $(|\mathbf{N}| + |\mathbf{G}|) \times |\Omega| + 1$  temporally aggregated subproblems, which are solved in parallel across assets and scenarios via consensus ADMM. Upon convergence of ADMM, determined according to the residual-based terminal condition of [21], the solution of the aggregated model is employed to compute  $F^{\text{UB}}$  and  $F^{\text{LB}}$ . If the relative difference between these bounds falls below the threshold  $\epsilon^{\text{thr}}$ , the algorithm terminates; otherwise  $\zeta$ ,

**Algorithm 1** Performance-Guaranteed Distributed Stochastic Predictive Control with A Posteriori Time Series Aggregation

---

**Input:**  $\beta$ ,  $\{ \theta_{n,\omega}^{\text{s}}, \theta_{g,\omega}^{\text{th}} \}_{n \in \mathbf{N}, g \in \mathbf{G}, \omega \in \Omega}$ ,  $\gamma$ ,  $\rho^0$ ,  $\epsilon^{\text{thr}}$ ,  $\zeta^0$ ,  $J$ ,  $I$ .

**Output:** Bounds  $F^{\text{UB}*}$  and  $F^{\text{LB}*}$ , and control actions  $\bar{\mathbf{u}}_0^*$ .

- 1:  $j \leftarrow 0$ ,  $\zeta^j \leftarrow \zeta^0$ ;
- 2: *Higher layer - Temporal aggregation:*
- 3: **while**  $100 \left| \frac{F^{\text{UB}^{j+1}} - F^{\text{LB}^{j+1}}}{F^{\text{UB}^{j+1}}} \right| > \epsilon^{\text{thr}}$  and  $j < J$  **do**
- 4: Perform TSA as detailed in Subsection II-E, using  $\zeta^j$  and the average marginal costs across scenarios from the previous MPC iteration as features;
- 5:  $i \leftarrow 0$ ,  $\rho \leftarrow \rho^0$ ,  $\{ \bar{p}_{n,\omega}^{\text{s}^0} \leftarrow \mathbf{0}^{2R}, \bar{p}_{g,\omega}^{\text{th}^0} \leftarrow \mathbf{0}^R, \hat{\lambda}_{n,\omega}^{\text{s}^0} \leftarrow \mathbf{0}^{2R}, \tilde{\lambda}_{n,\omega}^{\text{s}^0} \leftarrow \mathbf{0}^{2R}, \hat{\lambda}_{g,\omega}^{\text{th}^0} \leftarrow \mathbf{0}^R, \tilde{\lambda}_{g,\omega}^{\text{th}^0} \leftarrow \mathbf{0}^R, \forall n, \forall g, \forall \omega \}$ ;
- 6: *Lower layer - Consensus ADMM:*
- 7: **while** the residual-based terminal condition from [21] is not satisfied and  $i < I$  **do**
- 8:  $\{ \mathbf{z}^{\text{b}^{i+1}}, \mathbf{z}_{n,\omega}^{\text{s}^{i+1}}, \tilde{p}_{g,\omega}^{\text{th}^{i+1}} \} \leftarrow$  Solve (16)–(18);
- 9:  $\{ \bar{p}_{n,\omega}^{\text{s}^{i+1}}, \bar{p}_{g,\omega}^{\text{th}^{i+1}} \} \leftarrow$  Solve (19)–(20);
- 10:  $\{ \hat{\lambda}_{n,\omega}^{\text{s}^{i+1}}, \tilde{\lambda}_{n,\omega}^{\text{s}^{i+1}}, \hat{\lambda}_{g,\omega}^{\text{th}^{i+1}}, \tilde{\lambda}_{g,\omega}^{\text{th}^{i+1}} \} \leftarrow$  Solve (21)–(24);
- 11: Residual-based adaptive update of  $\rho$  from [21];
- 12:  $i \leftarrow i + 1$ ;
- 13: **end while**
- 14:  $\bar{\mathbf{u}}_0^* \leftarrow$  Solve (13l), and  $\bar{F}^* \leftarrow$  Solve (12);
- 15:  $F^{\text{PRJ}} \leftarrow$  Solve the full-scale stochastic model (11) with  $\mathbf{u}_0 = \bar{\mathbf{u}}_0^*$ ;  $\triangleright$  In parallel  $\forall \omega$
- 16:  $F^{\text{LB}^{j+1}} \leftarrow \bar{F}^*$ , and  $F^{\text{UB}^{j+1}} \leftarrow \min(F^{\text{UB}^j}, F^{\text{PRJ}})$ ;
- 17:  $\zeta^{j+1} \leftarrow \gamma \zeta^j$ ;
- 18:  $j \leftarrow j + 1$ ;
- 19: **end while**
- 20: **return**  $F^{\text{UB}*} \leftarrow F^{\text{UB}^j}$ ,  $F^{\text{LB}*} \leftarrow F^{\text{LB}^j}$  and  $\bar{\mathbf{u}}_0^*$ ;

---

initialized to  $\zeta^0$ , is reduced by a positive factor  $\gamma < 1$ , and the algorithm iterates again. Being the result of a projection step, the control actions computed by Algorithm 1 at time  $t$ , denoted by  $\bar{\mathbf{u}}_0^*$ , are **feasible** for the full-scale model (11). As illustrated in Fig. 1, Algorithm 1 provides a formal performance guarantee by allowing the decision-maker to evaluate the achieved optimality gap (i.e., the relative difference between upper and lower bounds) at each iteration.

### III. SIMULATION RESULTS AND DISCUSSION

This section presents the case study (Subsection III-A) and discusses the numerical results (Subsections III-B and III-C).

#### A. Case Study Description

We simulate the VPP energy dispatch over one year using a prediction horizon of 24 h and a sampling time of  $\Delta = 5$  min, i.e.,  $|\mathbf{K}| = 288$ . To ensure transparency and reproducibility, the VPP parameters are sampled from prescribed distributions.

For each storage unit, the minimum state of charge and charging/discharging power are set to 0 MWh and 0 MW, respectively. The energy capacity is drawn from a uniform distribution over [1, 5] MWh, while maximum charging/discharging

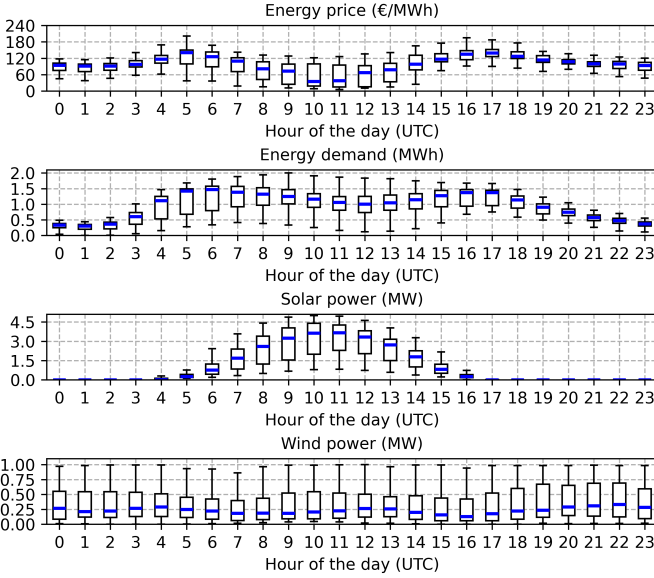


Fig. 3. Boxplots of the hourly uncertainty realization values. The box represents the interquartile range, the blue line indicates the median, and the whiskers extend to the minimum and maximum observations.

power limits are drawn uniformly from  $[0.1 \text{ MW}, \bar{E}_n^s / (1 \text{ h})]$ . The initial state is set to 0 MWh, and charging and discharging efficiencies are sampled uniformly from  $[0.7, 0.9]$  and  $[1/0.9, 1/0.7]$ , respectively. The reference states are  $\bar{E}_n^s / 2, \forall n$ .

For each thermal unit,  $\underline{P}_g^{\text{th}} = 0 \text{ MW}$ , the capacity is drawn uniformly from  $[0, 2] \text{ MW}$ , the ramp limit is  $\bar{P}_g^{\text{th}} / 6$ , and the parameters in (7) are  $\alpha_g = \frac{1}{2} (\bar{P}_g^{\text{th}})^{-2}$ ,  $\beta_g = (2\bar{P}_g^{\text{th}})^{-1}$ , and  $L_g^{\text{CO}_2} = 0.9$ . Thermal and storage operation costs are drawn uniformly from  $[30, 60]$  and  $[5, 15] \text{ €/MWh}$ , respectively. The cost of non-supplied energy is 5000 €/MWh, and deviations from storage reference states incur a cost of  $1 \text{ €/MWh}^2$ .

The uncertainty realizations are represented by scaled day-ahead energy prices, energy demand, and wind and solar power generation in Austria for 2024, obtained from the ENTSO-E Transparency Platform [38] and illustrated in Fig. 3. Scenarios are generated by perturbing these observations with Laplace-distributed noise  $\mathcal{L}(\mu, b_k)$ , where the scale parameter is set to  $b_k = 0.1k$  for  $k \in \mathbf{K}$ , reflecting the progressive growth of forecast uncertainty over the MPC prediction horizon. For each scenario, the location parameter  $\mu$  is sampled uniformly over  $[-0.05, 0.05]$ , introducing a scenario-specific bias.

If not otherwise specified, in Algorithm 1 we set  $\gamma = 0.9$ ,  $\rho^0 = 4$ ,  $\epsilon^{\text{thr}} = 1\%$ ,  $\zeta^0 = 2$ ,  $J = 10$ , and  $I = 500$ . The simulations are performed on an Intel i7 CPU with 32GB of RAM using Gurobi 12.0.1.

### B. Clustering Based on the Marginal Cost

As demonstrated in [31], exact temporal aggregation, i.e., zero error between the aggregated and full-scale models, is achieved when TSA yields an aggregated model that preserves the active constraints of the full-scale model. In (11), the marginal costs serve as an effective indicator of constraint activation over time: variations in these dual variables reflect changes in the marginal generating units and thus implicitly

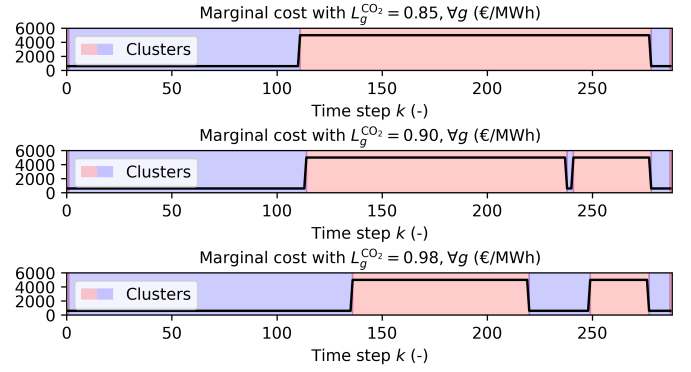


Fig. 4. Clusters obtained using marginal costs as features for TSA in the dispatch of thermal and solar power units under varying emission limits.

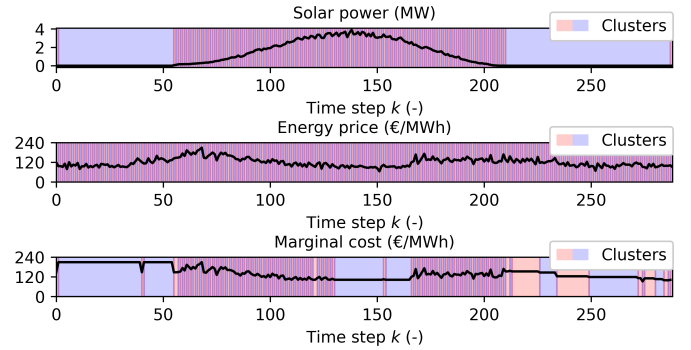


Fig. 5. Clusters obtained using different features (solar power, prices, or marginal costs) for TSA in the dispatch of storage and solar power units.

encode the activation of dispatch constraints. To illustrate the potential benefits of using marginal costs as clustering features for TSA, we consider the following examples.

We first examine a deterministic dispatch model ( $|\Omega| = 1$ ), comprising 10 thermal units. As shown in Fig. 4, applying the sliding window clustering technique of Subsection II-E with similarity threshold  $\zeta = 0$  and marginal costs as features, yields distinct sets of clusters depending on the emission limit parameters  $L_g^{\text{CO}_2}$ . Specifically, 5 to 7 clusters are identified (including the singleton clusters corresponding to the first and last hours in  $\mathbf{K}$ ), **enabling exact aggregation**, while reducing the temporal dimension by two orders of magnitude relative to the original 288 time periods. More importantly, Fig. 4 shows that the clusters yielding exact TSA vary with the structural properties of the dispatch model (here, the emission limit parameters), even when the input time series (scenarios) are identical. This is captured when performing TSA based on the marginal costs, whereas conventional a priori TSA methods, which rely solely on input time series analysis, generally fail.

Fig. 5 evaluates our TSA method under different feature selections for a deterministic dispatch model with 10 storage units. Using solar generation as a clustering feature yields a 30% aggregated model error, whereas energy prices provide no temporal reduction. In contrast, our marginal-cost-based TSA achieves exact aggregation with 137 clusters (52% reduction in the temporal dimension). Compared to the thermal-only case in Fig. 4, a larger number of clusters is required, reflecting the complexity induced by the intertemporal storage constraints.

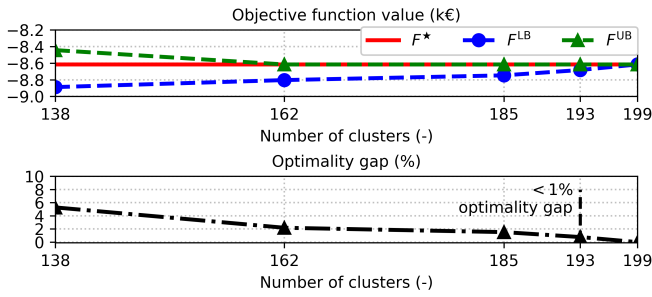


Fig. 6. Example of objective function bounds computed using Algorithm 1.

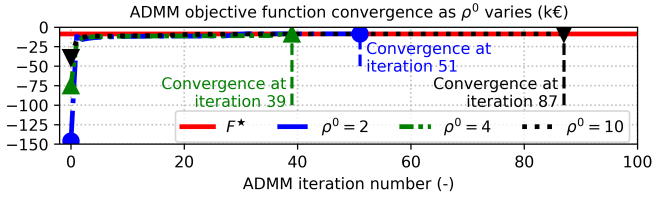


Fig. 7. Example of ADMM convergence within Algorithm 1 as  $\rho^0$  varies.

### C. Performance Evaluation of the Proposed Controller

An example of the objective function bounds computed by Algorithm 1 is shown in Fig. 6, for a dispatch problem with  $|\mathcal{N}| = |\mathcal{G}| = |\mathcal{Q}| = 50$ . The full-scale optimal objective value is reported solely for reference, as it is not required by the algorithm. The bounds are iteratively tightened, achieving an optimality gap of  $\sim 5\%$  with 138 clusters, and converging to a gap below 1% (i.e., over 99% accuracy relative to the full-scale controller) with 193 clusters ( $\sim 33\%$  reduction in the temporal dimension). Within Algorithm 1, the aggregated model is solved via consensus ADMM. Its convergence rate for different initial values of  $\rho$  is reported in Fig. 7, highlighting the well-known sensitivity of ADMM to parameter tuning [21]. An example of VPP dispatch obtained using Algorithm 1 is shown in Fig. 8 for an MPC iteration starting at midnight. Despite the simultaneous temporal aggregation and asset-scenario decomposition, our controller recovers the full-scale optimal control actions, dispatching the VPP flexibility units to meet energy demand with zero non-supplied energy.

Finally, Table II reports the average number of clusters  $|\mathcal{R}|$  and runtime of Algorithm 1 over MPC iterations, compared with full-scale MPC, as the optimality gap  $\epsilon^{\text{thr}}$  and the number of assets and scenarios vary. For small problem instances, Algorithm 1 may underperform relative to full-scale MPC (see the third row), yet it reduces runtime by up to 53% for  $\epsilon^{\text{thr}} = 1\%$  and 75% for  $\epsilon^{\text{thr}} = 5\%$  as the problem size grows. Crucially, it recovers tractability, where full-scale MPC fails to compute the dispatch within the available control time (5 min).

## IV. CONCLUSION AND FUTURE WORK

This paper addresses the real-time energy dispatch of a VPP formulated as a stochastic MPC problem. Owing to multiple sources of uncertainty, nonlinear dynamics, and several coupling constraints, solving the problem at full scale rapidly becomes intractable as the dispatch horizon, number of scenarios, and number of DERs increase. To overcome

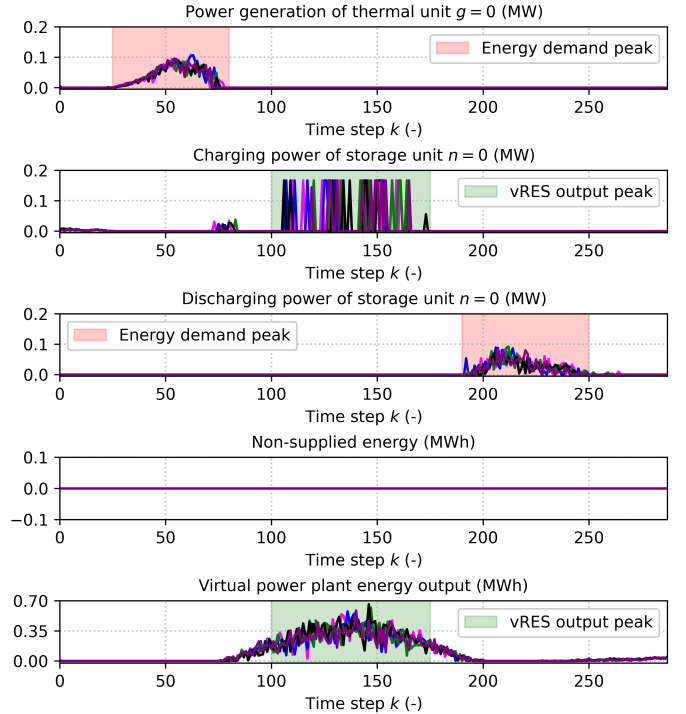


Fig. 8. Example of energy dispatch obtained using Algorithm 1 for the first storage unit ( $n = 0$ ) and the first thermal unit ( $g = 0$ ) of the VPP, shown for 5 randomly selected scenarios from a set with 50 scenarios.

TABLE II  
COMPUTATIONAL PERFORMANCE OF ALGORITHM 1 IN COMPARISON WITH FULL-SCALE MPC (FS-MPC) AS  $|\mathcal{Q}|$ ,  $|\mathcal{N}|$  AND  $|\mathcal{G}|$  INCREASE. RELATIVE RUNTIME DIFFERENCES ARE SHOWN IN **BOLD** IN BRACKETS, AND INTRACTABLE FS-MPC INSTANCES ARE HIGHLIGHTED IN **RED**.

$ \mathcal{Q} $	$ \mathcal{N} $	$ \mathcal{G} $	FS-MPC runtime (s)	$\epsilon^{\text{thr}}$	Algorithm 1	
					Avg. $ \mathcal{R} $	Avg. runtime (s)
50	50	50	46.9	1%	198.8	37.1 (−21%)
				5%	141.1	24.6 (−48%)
100	50	50	122.6	1%	199.0	92.1 (−25%)
				5%	138.6	57.9 (−53%)
50	100	100	148.2	1%	201.6	157.3 (+6%)
				5%	148.1	130.9 (−12%)
50	200	100	<b>356.5</b>	1%	212.3	276.1 (−23%)
				5%	166.9	189.7 (−47%)
50	100	200	<b>388.6</b>	1%	200.4	274.2 (−29%)
				5%	148.7	186.3 (−52%)
200	50	50	<b>433.8</b>	1%	202.8	205.5 (−53%)
				5%	108.0	109.1 (−75%)

this limitation, we propose a novel control scheme integrating MPC with TSA and distributed optimization to simultaneously reduce the temporal, asset, and scenario dimensions of the problem. Notably, the controller employs a closed-loop, a posteriori TSA method that exploits dual information, specifically marginal cost estimates, to refine temporal aggregation, in contrast to traditional TSA methods that rely solely on input time series analysis. Crucially, the controller embeds a rigorous performance guarantee in the form of theoretically validated bounds on its approximation error relative to full-scale MPC. Numerical results show that the proposed controller reduces runtime by over 50% relative to full-scale MPC and, more importantly, restores tractability where full-scale MPC proves computationally intractable. Future work

will incorporate transmission constraints, additional nonlinear dynamics and power flow constraints in the dispatch model.

#### ACKNOWLEDGMENTS

Funded by the European Union (ERC, NetZero-Opt, 101116212). Views and opinions expressed are however those of the authors only and do not necessarily reflect those of the European Union or the European Research Council. Neither the European Union nor the granting authority can be held responsible for them.

#### REFERENCES

- [1] M. Bahloul, L. Breathnach, and S. Khadem, "Residential virtual power plant control: A novel hierarchical multi-objective optimization approach," *IEEE Trans. Smart Grid*, vol. 16, no. 2, pp. 1301–1313, Mar. 2025.
- [2] X. Wei, J. Liu, Y. Xu, and H. Sun, "Virtual power plants peer-to-peer energy trading in unbalanced distribution networks: A distributed robust approach against communication failures," *IEEE Trans. Smart Grid*, vol. 15, no. 2, pp. 2017–2029, Mar. 2024.
- [3] H. Golpîra and B. Marinescu, "Enhanced frequency regulation scheme: An online paradigm for dynamic virtual power plant integration," *IEEE Trans. Power Syst.*, vol. 39, no. 6, pp. 7227–7239, Nov. 2024.
- [4] N. Naval and J. M. Yusta, "Virtual power plant models and electricity markets - A review," *Renew. Sustain. Energy Rev.*, vol. 149, pp. 111393, Oct. 2021.
- [5] J. Naughton, H. Wang, M. Cantoni, and P. Mancarella, "Co-optimizing virtual power plant services under uncertainty: A robust scheduling and receding horizon dispatch approach," *IEEE Trans. Power Syst.*, vol. 36, no. 5, pp. 3960–3972, Sept. 2021.
- [6] A. Bolzoni, A. Parisio, R. Todd, and A. J. Forsyth, "Optimal virtual power plant management for multiple grid support services," *IEEE Trans. Energy Convers.*, vol. 36, no. 2, pp. 1479–1490, June 2021.
- [7] D. Rosewater, R. Baldick, and S. Santoso, "Risk-averse model predictive control design for battery energy storage systems," *IEEE Trans. Smart Grid*, vol. 11, no. 3, pp. 2014–2022, May 2020.
- [8] L. Santosuosso, S. Camal, F. Liberati, A. Di Giorgio, A. Michiorri, and G. Kariniotakis, "Stochastic economic model predictive control for renewable energy and ancillary services trading with storage," *Sustain. Energy Grids Netw.*, vol. 38, pp. 101373, Jun. 2024.
- [9] J. He, C. Shi, T. Wei, and D. Jia, "Stochastic model predictive control of hybrid energy storage for improving AGC performance of thermal generators," *IEEE Trans. Smart Grid*, vol. 13, no. 1, pp. 393–405, Jan. 2022.
- [10] Z. Zhao et al., "Distributed robust model predictive control-based energy management strategy for islanded multi-microgrids considering uncertainty," *IEEE Trans. Smart Grid*, vol. 13, no. 3, pp. 2107–2120, May 2022.
- [11] Y. Shen, W. Wu, and S. Sun, "Stochastic model predictive control based fast-slow coordination automatic generation control," *IEEE Trans. Power Syst.*, vol. 39, no. 3, pp. 5259–5271, May 2024.
- [12] L. A. Roald, D. Pozo, A. Papavasiliou, D. K. Molzahn, J. Kazempour, and A. J. Conejo, "Power systems optimization under uncertainty: A review of methods and applications," *Elect. Power Syst. Res.*, vol. 214, pp. 108725, Jan. 2023.
- [13] Y. Zhang, F. Liu, Z. Wang, Y. Su, W. Wang, and S. Feng, "Robust scheduling of virtual power plant under exogenous and endogenous uncertainties," *IEEE Trans. Power Syst.*, vol. 37, no. 2, pp. 1311–1325, Mar. 2022.
- [14] H. Han, H. Zhang, J. Yang, and H. Su, "Distributed model predictive consensus control for stable operation of integrated energy system," *IEEE Trans. Smart Grid*, vol. 15, no. 1, pp. 381–393, Jan. 2024.
- [15] L. Santosuosso, "Distributed stochastic optimization for operating complex virtual power plants: Leveraging cascaded run-of-the-river hydropower flexibility for renewable energy integration," Ph.D. dissertation, Université Paris Sciences et Lettres, Paris, France, 2025.
- [16] C. Contreras, A. Triviño, and J. A. Aguado, "Distributed model predictive control for voltage coordination of large-scale wind power plants," *Int. J. Electr. Power Energy Syst.*, vol. 143, pp. 108436, Dec. 2022.
- [17] R. Halvgaard, L. Vandenberghe, N. K. Poulsen, H. Madsen, and J. B. Jørgensen, "Distributed model predictive control for smart energy systems," *IEEE Trans. Smart Grid*, vol. 7, no. 3, pp. 1675–1682, May 2016.
- [18] D. Zhu and G. Hug, "Decomposed stochastic model predictive control for optimal dispatch of storage and generation," *IEEE Trans. Smart Grid*, vol. 5, no. 4, pp. 2044–2053, July 2014.
- [19] K. Baker, J. Guo, G. Hug, and X. Li, "Distributed MPC for efficient coordination of storage and renewable energy sources across control areas," *IEEE Trans. Smart Grid*, vol. 7, no. 2, pp. 992–1001, Mar. 2016.
- [20] E. Rezaei, H. Dagdougui, and M. Rezaei, "Distributed stochastic model predictive control for peak load limiting in networked microgrids with building thermal dynamics," *IEEE Trans. Smart Grid*, vol. 13, no. 3, pp. 2038–2049, May 2022.
- [21] S. Boyd, N. Parikh, E. Chu, B. Peleato, and J. Eckstein, "Distributed optimization and statistical learning via the alternating direction method of multipliers," *Found. Trends Mach. Learn.*, vol. 3, no. 1, pp. 1–122, Nov. 2011.
- [22] C. Feng, K. Zheng, Y. Zhou, P. Palensky, and Q. Chen, "Update scheduling for ADMM-based energy sharing in virtual power plants considering massive prosumer access," *IEEE Trans. Smart Grid*, vol. 14, no. 5, pp. 3961–3975, Sept. 2023.
- [23] C. J. López-Salgado, O. Añó, and D. M. Ojeda-Esteybar, "Stochastic unit commitment and optimal allocation of reserves: A hybrid decomposition approach," *IEEE Trans. Power Syst.*, vol. 33, no. 5, pp. 5542–5552, Sept. 2018.
- [24] Y. Jia, P. Yong, C. Li, K. Meng, Z. Y. Dong, and C. Sun, "An ADMM-based resilient distributed economic MPC algorithm for frequency restoration and economic dispatch in networked microgrids," *IEEE Trans. Ind. Appl.*, early access, Oct. 2025.
- [25] L. Santosuosso, S. Camal, A. Lett, G. Bontron, J. Kazempour, and G. Kariniotakis, "A scenario-spatial decomposition approach with a performance guarantee for the combined bidding of cascaded hydropower and renewables," *IEEE Trans. Power Syst.*, early access, Nov. 2025.
- [26] H. Teichgraber and A. R. Brandt, "Time-series aggregation for the optimization of energy systems: Goals, challenges, approaches, and opportunities," *Renew. Sustain. Energy Rev.*, vol. 157, pp. 111984, Apr. 2022.
- [27] C. Zhang and R. Li, "A novel closed-loop clustering algorithm for hierarchical load forecasting," *IEEE Trans. Smart Grid*, vol. 12, no. 1, pp. 432–441, Jan. 2021.
- [28] T. Schütz, M. H. Schraven, M. Fuchs, P. Remmen, and D. Müller, "Comparison of clustering algorithms for the selection of typical demand days for energy system synthesis," *Renew. Energy*, vol. 129, pp. 570–582, Dec. 2018.
- [29] Y. Liu, R. Sioshansi, and A. J. Conejo, "Hierarchical clustering to find representative operating periods for capacity-expansion modeling," *IEEE Trans. Power Syst.*, vol. 33, no. 3, pp. 3029–3039, May 2018.
- [30] Y. Zhang, V. Cheng, D. S. Mallapragada, J. Song, and G. He, "A model-adaptive clustering-based time aggregation method for low-carbon energy system optimization," *IEEE Trans. Sustain. Energy*, vol. 14, no. 1, pp. 55–64, Jan. 2023.
- [31] S. Wogrin, "Time series aggregation for optimization: One-size-fits-all?," *IEEE Trans. Smart Grid*, vol. 14, no. 3, pp. 2489–2492, May 2023.
- [32] M. Sun, F. Teng, X. Zhang, G. Strbac, and D. Pudjianto, "Data-driven representative day selection for investment decisions: A cost-oriented approach," *IEEE Trans. Power Syst.*, vol. 34, no. 4, pp. 2925–2936, July 2019.
- [33] S. Pineda and J. M. Morales, "Chronological time-period clustering for optimal capacity expansion planning with storage," *IEEE Trans. Power Syst.*, vol. 33, no. 6, pp. 7162–7170, Nov. 2018.
- [34] S. Deml, A. Ulbig, T. Borsche, and G. Andersson, "The role of aggregation in power system simulation," in *2015 IEEE Eindhoven PowerTech*, Eindhoven, Netherlands, 2015, pp. 1–6.
- [35] H. Teichgraber and A. R. Brandt, "Clustering methods to find representative periods for the optimization of energy systems: An initial framework and comparison," *Appl. Energy*, vol. 239, pp. 1283–1293, Apr. 2019.
- [36] L. Santosuosso, B. Klinz, and S. Wogrin, "What are we clustering for? Establishing performance guarantees for time series aggregation in generation expansion planning," *arXiv preprint*, 2025. [Online]. Available: <https://arxiv.org/abs/2510.09357>.
- [37] H. Moghimi, A. Ahmadi, J. Aghaei, and A. Rabiee, "Stochastic techno-economic operation of power systems in the presence of distributed energy resources," *Int. J. Electr. Power Energy Syst.*, vol. 45, no. 1, pp. 477–488, Feb. 2013.
- [38] L. Hirth, J. Mühlenpfordt, and M. Bulkeley, "The ENTSO-E Transparency Platform—A review of Europe's most ambitious electricity data platform," *Appl. Energy*, vol. 225, pp. 1054–1067, Sept. 2018.